Comparison of energy fluxes at the land surface-atmosphere interface in an Alpine valley as simulated with different models

G. Grossi, L. Falappi

Hydrology and Earth System Sciences, 7(6), *920–936* (2003) © EGU

Hydrology & Earth System Sciences

Comparison of energy fluxes at the land surface-atmosphere interface in an Alpine valley as simulated with different models

G. Grossi and L. Falappi

Università degli Studi di Brescia, Dipartimento di Ingegneria Civile, Via Branze 38, I-25123 Brescia, Italy

E-mail for corresponding author: grossig@ing.unibs.it

Abstract

Within the framework of a research project coupling meteorological and hydrological models in mountainous areas a distributed Snow/Soil-Vegetation-Atmosphere Transfer model was developed and applied to simulate the energy fluxes at the land surface – atmosphere interface in an Alpine valley (Toce Valley - North Italy) during selected flood events in the last decade. Energy fluxes simulated by the distributed energy transfer model were compared with those simulated by a limited area meteorological model for the event of June 1997. The differences in the spatial and temporal distribution of the energy fluxes simulated by the two models are outlined. The Snow/Soil-Vegetation-Atmosphere Transfer model was also applied to simulate the energy fluxes at the land surface-atmosphere interface for a single cell, assumed to be representative of the Siberia site (Toce Valley), where a micro-meteorological station was installed and operated for 2.5 months in autumn 1999. The Siberia site is very close to the Nosere site, where a standard meteorological station was measuring precipitation, air temperature and humidity, global and net radiation and wind speed during the same special observing period. Data recorded by the standard meteorological station were used to force the energy transfer model and simulate the point energy fluxes at the Siberia site, while turbulent fluxes observed at the Siberia site were used to derive the latent heat flux from the energy balance equation. Finally, the hourly evapotranspiration flux computed by this procedure was compared to the evapotranspiration flux simulated by the energy transfer model.

Keywords : energy exchange processes, land surface-atmosphere interactions, turbulent fluxes

Introduction

Recently, the hydrological modelling community has addressed the conceptual description of the energy and mass exchange processes occurring at the land surface-atmosphere interface. In fact, these processes affect the hydrological cycle and the production of runoff within the basin, especially in mountain areas where the melting of snow or ice covering the soil is dominated by these energy exchange processes. Indeed, during flood events, most of which are forced by heavy precipitation, the soil can play the role of an important humidity and heat source affecting the formation of storm cells and snow or ice melting can contribute to the generation of runoff. Therefore, both the water cycle on the surface and the dynamics of the atmospheric system are sensitive to exchange processes occurring at the interface.

Meteorological models, nowadays, forecast meteorological variable fields at the soil surface at high spatial (3×3 km²) and temporal (1 h) resolutions, quite close to those needed for an accurate simulation of the hydrological response of the basin. Recent advances in hydrology are addressed to the explicit representation of the soil-atmosphere interactions, at a spatial resolution ranging from some tens of metres to a maximum of 1 km. In Alpine valleys, for example, the meteorological conditions leading to flood events are strongly affected by the complex orography, the spatial variability of which can hardly be accommodated in a digital elevation model with a resolution of less than 1 km. A mathematical model describing in detail both the surface water system and the atmosphere would be far too expensive and time consuming for operational purposes. On the other hand promising results might derive from coupling detailed models of the two systems, using the output of the meteorological model as input to the hydrological model.

The EU funded RAPHAEL project (1998–2000) (Bacchi

and Ranzi, 2003) investigated the limits and potentials of coupling meteorological and hydrological models at the regional scale to improve flood forecasting in complex mountain catchments. It had two target areas: the Ammer catchment, located in the German Alps, and the Swiss-Italian Ticino-Toce catchment. One of the main objectives of RAPHAEL was "to improve techniques and tools for scale-adaptation of observed and simulated variables, with particular reference to the areal distribution of rainfall, snow cover and land-surface-atmosphere fluxes". In this perspective, for the characterisation of the hydrological response of the Toce catchment at the land surface–atmosphere interface, a distributed Snow/Soil-Vegetation-Atmosphere-Transfer model (SSVAT) model was developed and used to simulate the energy fluxes in the Toce Valley during selected flood events in the last decade.

The first part of the present work reports the analyses of areal energy fluxes, simulated for the event of June 1997 (TT4 event), for which the energy transfer fields were simulated by the meteorological model BOLAM (Buzzi *et al*., 1994; Malguzzi and Tartaglione, 1999). In fact, the comparison of the distribution of energy fluxes simulated by a meteorological and a hydrological model could outline discrepancies in the representation schemes adopted and in the physiographic parameters used by each algorithm.

The international Mesoscale Alpine Project (MAP) is also addressing research in this direction, with particular attention to intense rainfall field forecasting. Italy is frequently affected by heavy precipitation because of the local interaction of the atmospheric circulation with the Alps. The intense precipitations are due to the mesoscale interaction of the atmospheric circulation with the Alps: air masses rich in humidity, loaded during their passage over the Mediterranean Sea or the Atlantic Ocean, are lifted and cooled. To study the phenomena at the mesoscale in this region, within the MAP framework a Special Observation Period (SOP'99) was planned for Autumn 1999 (Bougeault *et al*., 2001). In Italy, the valley drained by the Toce river was chosen as the target area: during MAP-SOP'99, an intensive field campaign, focused on hydrological and meteorological data collection, was effected from 1 September to 15 November 1999 (Ranzi and Bacchi, 2000; Falappi *et al*., 2001a,b; Grossi *et al.*, 2001).

A micro-meteorological station measuring turbulent fluxes of heat and momentum was installed near Domodossola, very close to a standard meteorological station measuring precipitation, air temperature and humidity, global and net radiation and wind speed. Data recorded by the standard meteorological station were used as input to the SSVAT model to simulate the energy exchange processes at a single cell and compare them with those derived from observations recorded at the micro-meteorological station. Results of this comparison are reported and discussed in the second part of the work.

Model description

The model used is an improvement of the distributed energy-balance snowmelt model first developed by Ranzi and Rosso (1991) and Grossi (1996); it had already been applied to some mountain areas in the Alps (Ranzi and Rosso, 1990) and in the Rocky Mountains (Grossi *et al*., 1995). It is assumed that topography, land use and soil properties, snow and vegetation cover data are represented on a raster grid. For each grid cell it provides a solution of the two-dimensional energy balance equation and the mass balance, including melt, refreezing and snowmelt flux in the vertical direction. The meteorological information needed for its application includes precipitation, air temperature, wind speed, humidity, downwelling shortwave radiation and surface air pressure at 1 h temporal resolution.

Different extrapolation procedures are applied to represent the spatial variability of these quantities. Both humidity and wind speed are assumed to be constant in space, while the air pressure changes with altitude assuming a hydrostatic law. Precipitation is corrected and distributed as a function of the solid and liquid fractions, estimated on the basis of the air temperature according to the scheme discussed in Ranzi *et al*. (1999). A linear altitudinal trend is assumed for hourly air temperature, the slope being the vertical lapse rate, *GT*.

A more detailed scheme is applied to distribute shortwave radiation, which can vary significantly due to changes in slope and aspect, the presence of topographic shadow and interaction with the terrain (Obled and Harder, 1978; Bach and Braun, 1999). The solar radiation at the top of the atmosphere, computed at each time step, is attenuated by the atmosphere; the beam and diffuse radiation under clear-sky conditions are also computed, their sum being R_c. Then, the fraction of diffuse radiation under non-clear sky conditions is estimated on the basis of the actual measurements, R_m, assuming that clouds with *tclo* transmissivity are such that all the solar radiation is diffused towards the Earth's surface. The fraction *cloudi*, which can be considered a cloudiness index, is then set equal to the ratio of the difference R_c–R_m and the maximum difference that can be, in theory, observed, $(1- tclo)R_c$. In all weather conditions, the diffuse component R_d at the radiometric station is computed as a sum of the diffuse sky radiation, $R_{s,d}$, that depends on the cloudiness index, and the radiation reflected from the surrounding terrain with albedo α and view factor V_t. Beam radiation at the measurement site, R_b,

is finally computed as the difference between measured total radiation and the estimated diffuse component, $R_b=R_m-R_d$.

THE ENERGY BALANCE FOR SNOW-COVERED AREAS

The snowpack is assumed to consist of two layers: the surface layer (with a constant maximum depth of 10 cm) and the remainder; the state variables used to describe the snowpack physics are depth, density, temperature, water equivalent and the liquid water content. For each cell, the snow depth *hs* is updated at each time step by solving the mass balance equation. The density of snow also changes at each time step; it is computed by solving the continuity equation, assuming compaction of snow and percolation with a celerity computed after Colbeck and Anderson (1982).

The energy balance is computed for each of the two layers of the snowpack. The energy gained from the snowpack or available for melting (or refreezing) of a mass M per unit time, results from exchange fluxes of heat by conduction from the ground, H_g, net shortwave and longwave irradiance, R, evaporation (or condensation), H_l, turbulent transport, H_s, and advection, H_a:

$$\frac{\partial}{\partial t}\left(C_{pi}\rho_s T_s\right)+M\cdot L_f = H_g + R + H_l + H_s + H_a$$

Clear-sky snow albedo is computed as a function of season and snow metamorphosis. Cloudiness or the presence of diffuse radiation implies an increase in snow albedo that is modified accordingly. Finally, shortwave radiation is computed as the difference between total downwelling and reflected radiation.

The longwave radiation emitted by the atmosphere and the snow cover is computed by the Stefan- Boltzmann law. While the snow cover is treated as a 'grey' body with an emissivity of 0.99, the actual emissivity of air is computed as a function of air temperature and vapour pressure. To account for the effect of cloudiness, the air emissivity is also weighted with the cloudiness index; the atmosphere is also treated as a black body under overcast conditions.

Boundary layer theory is applied to evaluate the sensible and the latent heat fluxes. The algorithm relies on the hypothesis that the ratios of the transfer coefficients of heat and momentum, K_h/K_m, and of moisture and momentum, K_e/K_m, are always equal to unity, a reasonable hypothesis for the air layers close to the snow surface during snowmelt. The advective heat on the snow surface is computed both for snowfall and for rainfall assuming a temperature of precipitation equal to the air temperature.

For the conductive term, the analytical solution that approximates the heat conduction into a layer of finite depth of some centimetres of snow with given thermal conductivity and diffusivity is used. The equation is solved through a finite difference procedure, on the basis of the initial and boundary conditions of the system: heat and water flux at the snow-air interface and the temperature at the soil-snow interface (T_g=0°C). The snow temperature T_s is finally computed as the ratio of the heat content and the heat capacity of the snow layer (product of the mass and the specific heat at constant pressure, C_p).

THE ENERGY BALANCE FOR SNOW-FREE AREAS

The interception process is described by a model similar to that of Rutter-Calder (Calder, 1990): it is assumed that inflows to the canopy storage are equal to the precipitation rate minus a constant 'free throughfall fraction', p. The drainage is related to the canopy storage via two parameters, b and k, while evaporation is assumed to be proportional to the current storage for water contents lower than the canopy capacity. Throughflow TF is computed as the excess of the accumulated interception storage to the capacity SI_{max}:

$$TF = \max(P_t + SI_t - EI_t - SI_{max}, 0)$$

where P_t is the precipitation amount in the current time step.

The value of SI_{max} is set on the basis of the known plant characteristics: the leaf area index, LAI, and the fraction of ground surface covered by canopy, F.

The interception storage SI, representing the current volume of water retained by the plant canopy, decreases as evaporation of intercepted water, EI, occurs at the potential rate (water surface). It depends on the volume of precipitation at the current time step and on evaporation and interception storage at the previous time step. The evaporation of the intercepted water is also set equal to the minimum value between the interception loss and the evaporation at the potential rate (EP) of the intercepted water at the same time step.

The potential transpiration from a dry vegetative surface, TP_d, with surface resistance r_s is calculated using a Penman-Monteith approach (Monteith, 1981):

$$TP_d = \frac{1}{\lambda}\frac{\Delta R_n + \rho c_p (e_s - e_d)/r_a}{\Delta + \gamma(1 + r_s/r_a)}$$

where λ is the latent heat of vaporisation, Δ is the gradient of saturated vapour pressure e_s versus air temperature T, R_n is the energy available for the process, ρ is the density of the air, c_p is the specific heat of the air at a constant pressure, e_s-e_d is the deficit of water vapour pressure, γ is the psychrometric constant, r_s and r_a are respectively the surface and the aerodynamic resistances. Potential evaporation (EP)

of the intercepted water is also computed by the Penman-Monteith formulation for a wet surface (assuming surface resistance $r_s = 0$).

The aerodynamic resistances to the water vapour diffusion are computed using the formulation:

$$r_a = \frac{\ln^2 [(z - d)/z_0]}{k^2 \cdot u_z}$$

where z is the height of wind speed measurements, z_0 is the surface roughness, d is the zero plane displacement, k is the von Karman constant (= 0.41), u_z is the wind speed at height z.

Following Wigmosta *et al*. (1994), the ratio of potential transpiration from a dry canopy and the potential wet canopy evaporation rate is found by dividing the two formulae:

$$TP_d / EP = \frac{\Delta + \gamma}{\Delta + \gamma(1 + r_s / r_a)}$$

The same ratio applies to the computation of the potential transpiration rate from partially wet vegetation, *TP*. It is proportional to the potential evaporation rate from wet surfaces, *EP*, diminished by the effective evaporation of intercepted water, *EI*:

$$TP = (EP - EI)\frac{\Delta + \gamma}{\Delta + \gamma(1 + r_s / r_a)}$$

To simulate the heat fluxes in snow-free areas, the code assumes a two layer scheme for the soil as well. For the upper layer, a simplified energy balance equation is solved to compute the soil surface temperature.

The heat flux towards the soil surface layer depends on the soil temperature profile $T_s(z)$ and on the soil conductivity λ, as assessed by the Fourier heat transfer law. Typical values of λ are 3.5 W/m/°C for granite and gneiss rocks and 0.85 W/m/°C for loamy soils at field capacity. The vertical coordinate z is positive downward, so that

$$H_g(z) = \lambda(z) \mathrm{d}T_s(z)/dz$$

The model assumes that a surface (upper) layer with depth z_s and thermal diffusivity α_s is sensitive to the diurnal temperature fluctuations $T_d(t)$. Below the depth z_s, the thermal regime and the heat fluxes in the deep rock layer, assumed semi-infinite, is sensitive only to the annual fluctuations of the air temperature T_m.

The regime of the mean daily temperature on the day d from the 1st of January, $T_m(H,d)$ is assumed sinusoidal with $\omega_\alpha = 2\pi/365$, amplitude A_m and mean annual temperature $T_m(H)$, depending on the altitude H. For a sinusoidal diurnal temperature cycle, with period $\tau = 24$ h and a time shift φ (generally about –12 h), amplitude A_d, and mean daily value $T_m(h,d)$ representing the upper boundary conditions for the surface soil layer, the expression of the temperature profile at depth z can be written as:

$$T_s(h,d,t,z) = T_m(h,d) + A_d \exp(-\gamma z) \sin[\omega_d(t+\varphi) - \gamma z]$$

The damping factor $\gamma = \sqrt{[\pi/(a\tau)]}$ is a function of the thermal diffusivity α_S. Typical values of α range from 0.36×10^{-6} $m^2\ s^{-1}$ for soils to 1.6×10^{-6} $m^2\ s^{-1}$ for rocks resulting in γ values of 9.5 and 5.3 m^{-1}, respectively. The depth of the surface layer z_s is taken equal to the depth at which diurnal fluctuations of air temperature are damped out to 1/10. Accordingly $z_s = 0.24$ m for a surface soil layer and $z_s = 0.43$ m for a rock layer.

The heat balance for the surface layer of depth z_s can now be written outlining the dependencies on air and soil temperature:

$$Cv\, z_s\, \mathrm{d}T/\mathrm{d}t = S_{io} + L_{io}(T_a, T_s) + H_l(e_a, e_s(T_s)) + H_s(T_a, T_s) + H_a + H_g(z_s)$$

where Cv is the volumetric specific heat of the soil layer ranging from 2.39×10^6 to 2.16×10^6 $J/m^3/°C$ for soil and rock, respectively. H_s, H_l, H_a, S_{io} and L_{io} are the net fluxes of sensible, latent and advective heat, shortwave and longwave radiation entering the soil layer respectively. For the daily conductive heat flux, the analytical solution in the case of a semi-infinite underlying rock layer forced by the annual thermal regime is:

$$Hg(d,zs) = -\sqrt{2\ \lambda\gamma A_m}\ e^{-\gamma zs} \sin(\omega_a d - \gamma z_s + \pi/4 - \pi/2)$$

Assuming now the period τ_a equal to 1 year, for a rock layer, γ turns out to be 0.28 m^{-1} and the exponent γz_s, needed to compute the thermal damping factor $e^{-\gamma zs}$ is equal to 0.067 and 0.121, respectively. With these values, the expression for the ground heat flux in the day d from the beginning of the year at the depth z_s, can be further defined:

$$Hg(d,z_s) = 13.7\ e^{-\gamma zs} \sin(\omega_a d - \gamma z_s - \pi/4)$$

The energy balance equation for the surface layer is highly nonlinear, for example due to the presence of the longwave net fluxes, *Lio*, depending on the fourth power of the air and soil temperatures. A finite difference numerical solution is chosen where the terms nonlinearly dependent on the unknown soil temperature $T_{s,t}$ are computed as a function of the soil temperature at the previous time step $T_{s,t-1}$.

Basin representation

A digital elevation model (DEM) with a spatial resolution of 250 m was used to simulate the energy exchange processes at the snow/soil/vegetation-atmosphere interface in the Toce River basin, above Candoglia (1532 km²). On the basis of the DEM, the boundaries of the Toce catchment and of its eight sub-basins have been extracted with the help of SDPP (Pilotti *et al*., 1996; see Fig. 1 and Table 1).

For each sub-basin, a representative meteorological station was chosen on the basis of data availability: humidity and wind speed data recorded at that station were assumed to be representative of the whole sub-basin, while air pressure, solar radiation and temperature were extrapolated according to the procedures described in the previous paragraph. For clear-sky days, the hourly altitude temperature gradient, GT_{cs}, exhibited a periodic and asymmetric behaviour, as already proposed by Ca' Zorzi and Dalla Fontana (1986) to

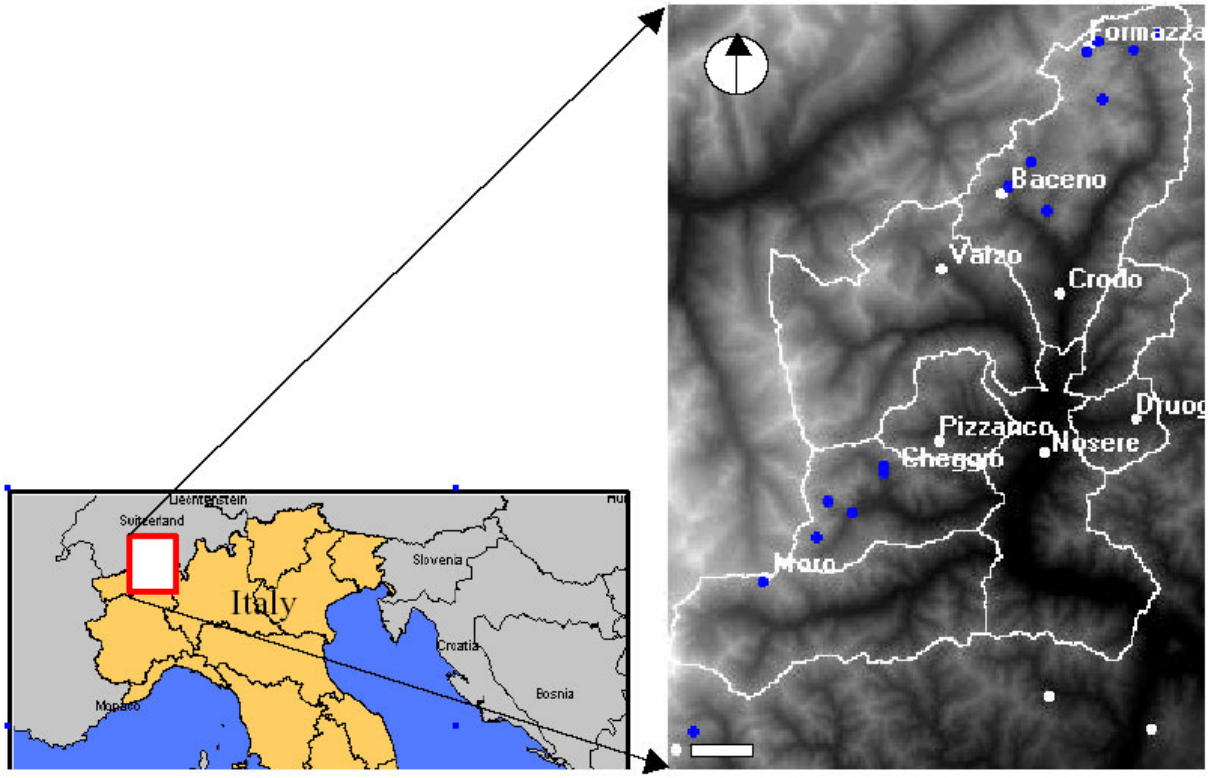

Fig. 1. *Boundaries of the eight sub-basins of the Toce catchment; white dots represent the automatic meteorological stations, blue dots indicate the snow gauges. The white bar indicates a 10 km distance.*

Table 1.The sub-basins of the Toce catchment and the meteorological stations selected for the representation of each meteorological variable. Toce at Candoglia* stands for the basin collecting runoff from the upstream ones.

	creek	*hydrometric station*	*area (km²)*	*precip.*	*air temp.*	*air hum.*	*wind sp.*	*solar rad.*	*air press.*
23	Toce	Pontemaglio	360.0	Baceno	Baceno	Baceno	Formazza	Nosere	Nosere
22	Isorno	Pontetto	70.5	Nosere	Nosere	Nosere	Nosere	Nosere	Nosere
24	Diveria	Crevoladossola	316.9	Varzo	Varzo	Varzo	Nosere	Nosere	Nosere
21	Melezzo	Masera	50.4	Druogno	Druogno	Druogno	Nosere	Nosere	Nosere
20	Bogna	Pontecaddo	81.4	Pizzanco	Pizzanco	Pizzanco	Nosere	Nosere	Nosere
25	Ovesca	Villadossola	145.1	Cheggio	Cheggio	Nosere	Moro	Nosere	Nosere
19	Anza	Piedimulera	257.1	Moro	Moro	Moro	Moro	Nosere	Nosere
28*	Toce	Candoglia*	250.7	Nosere	Nosere	Nosere	Nosere	Nosere	Nosere

describe the distribution of hourly air temperature. For overcast conditions. such a periodic behaviour was not observed and an average lapse rate, GT_{cc}, of 0.0052°C m^{-1} was estimated on the basis of the hourly data in the months of June 1996 and 1997 in the area of investigation. The temperature gradient in all weather conditions was finally computed as a weighted average of the overcast and the clear-sky temperature gradients, the weights being a function of the estimated cloudiness. A further temperature correction computed through an harmonic function of the average aspect of the terrain around each grid cell is also applied, with a scheme similar to that adopted by Schulla (1997).

To compute the heat conduction term at the land surface - atmosphere interface, the regime of the mean daily temperature is assumed sinusoidal as described above. For the Toce area, climatological studies (Biancotti *et al*., 1998) indicate that the amplitude A_m can be set equal to 10°C and the mean annual temperature can be computed as $T_m(H) = 12–0.0064(H–277)$, where H is expressed in metres.

Landuse, leaf area index and albedo maps derived from Landsat (30 × 30 m) satellite images (Bach and Braun, 1999) for the Toce catchment were resampled at 250 m and used to determine the presence and type of vegetation and the reflective properties of cells with no snow covering the ground.

Simulation of the areal energy fluxes during TT4 event (June 1997)

The shortwave and longwave radiation balance, latent and sensible heat fluxes at the land surface were simulated using the SSVAT scheme for the whole month of June 1997. The initial distribution of the snowpack water equivalent was estimated on the basis of the snow covered area derived from the NOAA image of 30 May 97 and of the snow depth monitored at snow gauges on 01 June 97. An 'internal' calibration and verification of the model was possible in two different ways:

(1) comparison of the areal extension of the snow cover simulated by the model for 12:00 UTC of the 15th of June and the areal extension of the snow cover estimated through the contemporary NOAA-AVHRR satellite image.
(2) comparison of point hourly snow depth observed in some snowgauges in the basin and the snow depth simulated by the model for the corresponding grid cell, 250 × 250 m in size

By resampling the derived remote image at a 250 m resolution, the number of grid cells covered by snow was 3517, while the model simulated a snow depth greater than 0 in 3044 cells: this yields a percentage error of –13%. Further comparison of snow height simulated and monitored for the whole month of June 1997 at the Passo del Moro gauge station (see Fig. 1), suggesting a good correlation between observed and simulated snowpack dynamics.

The spatial and temporal distributions of the simulated energy fluxes were analysed for the event of the 28th–30th June 1997 and a map of surface soil temperature computed for the time step 12:00 UTC of the 29th of June 1997 is shown in Fig. 2: values ranged from –5.2 to 28.3°C.

For a 24 h period in the middle of the TT4 event, the energy fluxes were also simulated by BOLAM with a 3.5 km resolution, applying a successive one-way nesting at resolutions of 35 of 10 km and of 3.5 km of mesh size. The 35 km BOLAM run used ECMWF 6 hourly operational analysis as initial and boundary conditions. BOLAM (BOlogna_Limited_Area_Model; Buzzi *et al.*, 1994) is a grid-point hydrostatic model with wind components u and v, potential temperature ϑ, specific humidity q, surface pressure p_s, as dependent variables. The vertical coordinate is terrain-following s, with variables distributed on a non-uniformly spaced Lorenz grid. The horizontal discretisation uses geographical coordinates, with latitudinal rotation, on an Arakawa-C grid. A fourth order diffusion term is added to all prognostic equations except in the tendency of p_s. A second order horizontal diffusion is applied to the divergence of horizontal velocity. The model has been tested and compared with a number of other mesoscale limited area models in the course of the COMPARE WMO Project. Recent model developments, tested and verified during the RAPHAEL project, are related to:

(i) modified new water cycle scheme, with parameterisation of the main microphysical processes and with explicit treatment and semi-Lagrangian advection and fall of five distinct hydrometeors, including ice phase condensates (cloud ice, snow and graupel);
(ii) implementation into the basic hydrostatic scheme of non-hydrostatic corrective terms;
(iii) modified convective parametrisation scheme, based on the Kain- Fritsch method (Benoit *et al*., 2000).

The spatial distribution of the shortwave radiation balance and of the turbulent fluxes simulated by the SSVAT model and the meteorological model for the same 24 hour period is shown in Fig. 3, reporting the maps of the total energy fluxes. The same legend categories were used for pictures referring to the same energy term, to outline which model showed the highest variability. The shortwave radiation

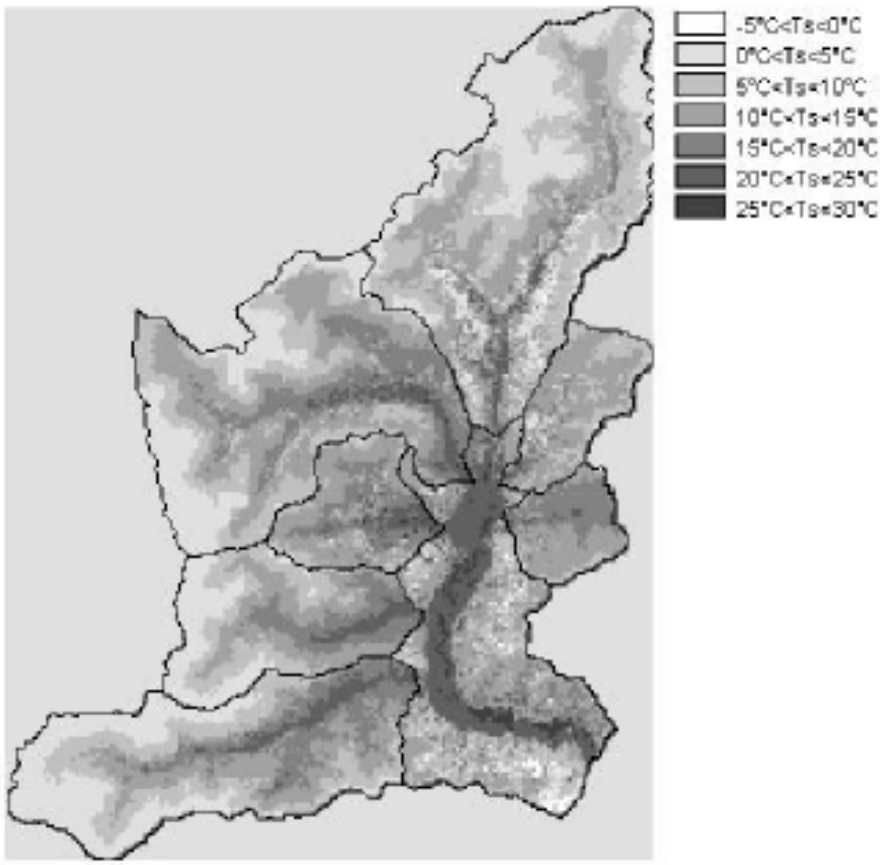

Fig. 2. *Distributed surface soil temperature simulated by SSVAT at 12:00 UTC of the 29th of June 1997, darker colour indicates higher temperature in the range [-5.2, 28.3] °C.*

balance distribution simulated by the meteorological model shows higher values and a higher variability than that provided by the SSVAT scheme. The same behaviour is obtained for the spatial distribution of the latent heat flux, while the opposite occurs for the sensible heat.

Figure 4 shows the hourly catchment average and standard deviation for each energy term simulated by the two models during the event: it is a lumped representation of the temporal dynamics of each energy term. Fluxes are positive downward, i.e. if the soil is gaining energy. Some descriptive statistics of the lumped energy fluxes series are summarised in Table 2: the average here is the spatial and temporal average of each energy flux. Higher values are characteristic of both the shortwave radiation balance and the latent heat flux (absolute values) simulated by the meteorological model, while the sensible heat flux is on average higher when simulated by the SSVAT model.

In the afternoon of 29th June, the meteorological model overestimates the shortwave fluxes (Fig. 4). This is likely due to an underestimation of cloudiness and has an impact on the other fluxes in the same hours. For instance the meteorological model assumes higher evaporation than the hydrological scheme. Moreover, the soil surface in the same hours was likely to be cooler than predicted by the meteorological model.

The MAP-SOP'99 experiment

To test the reliability of the SSVAT scheme to simulate the energy, as well as the turbulent energy fluxes, micro-meteorological observations recorded during SOP'99 at the Siberia site were used. The standard meteorological information needed for the application of the SSVAT model was provided by the observations recorded at the Domodossola site nearby.

The dataset used for the comparison experiment was, therefore, recorded by two different gauges, which are actually very close to each other, as indicated in Fig. 5. The geographical coordinates are reported in Table 3. Both the stations are in the bottom of the Toce Valley, the geographical axis of which is oriented along the NNE–SSW direction.

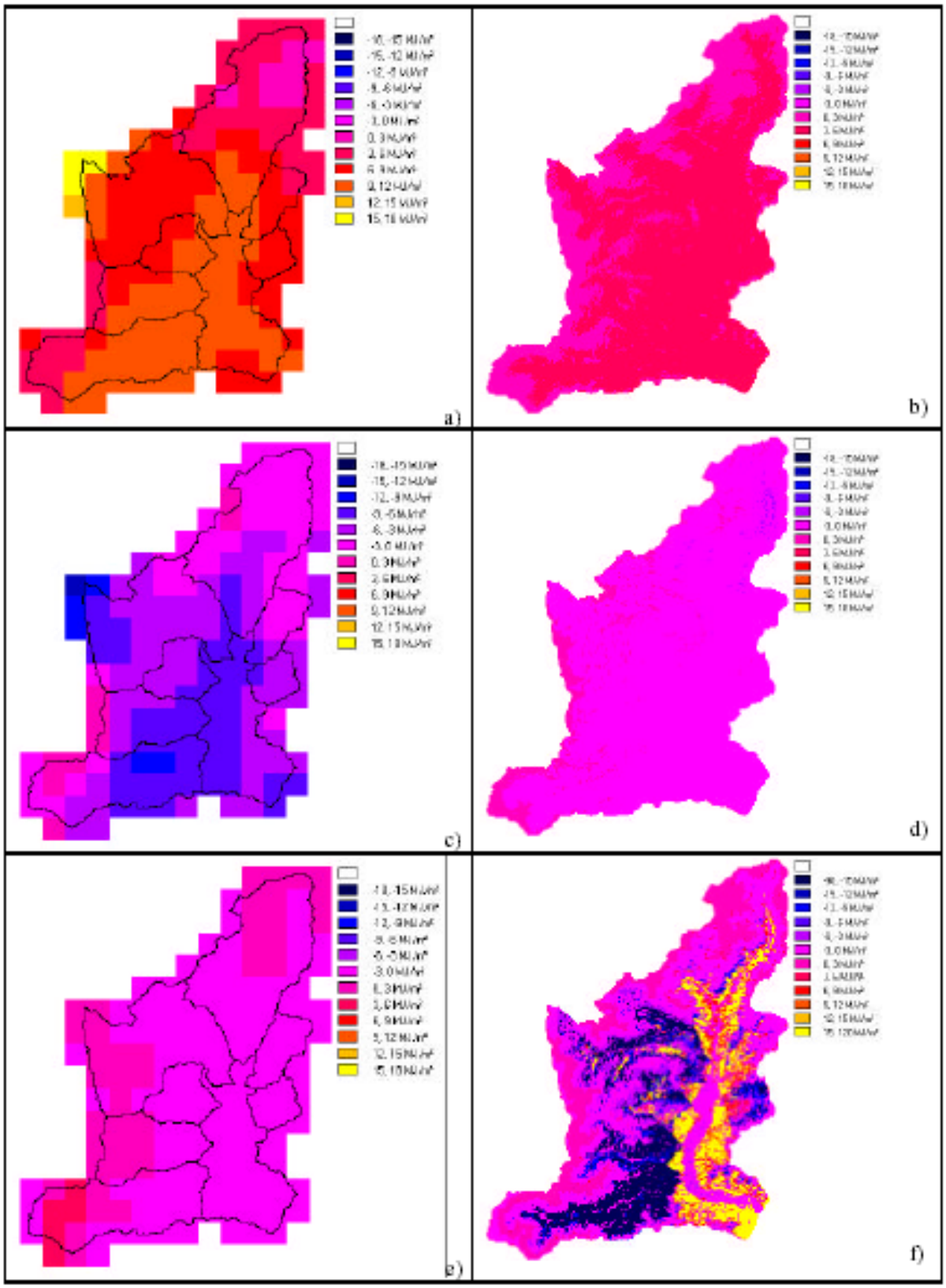

Fig. 3. *Distributed energy fluxes at the snow/soil surface simulated by BOLAM and SSVAT from 18:00 UTC of the 28th of June untill 18:00 UTC of the 29th of June 1997 (TT4 event): a) BOLAM and b) SSVAT shortwave radiation balance, c) BOLAM and d) SSVAT latent heat, e) BOLAM and f) SSVAT sensible heat.*

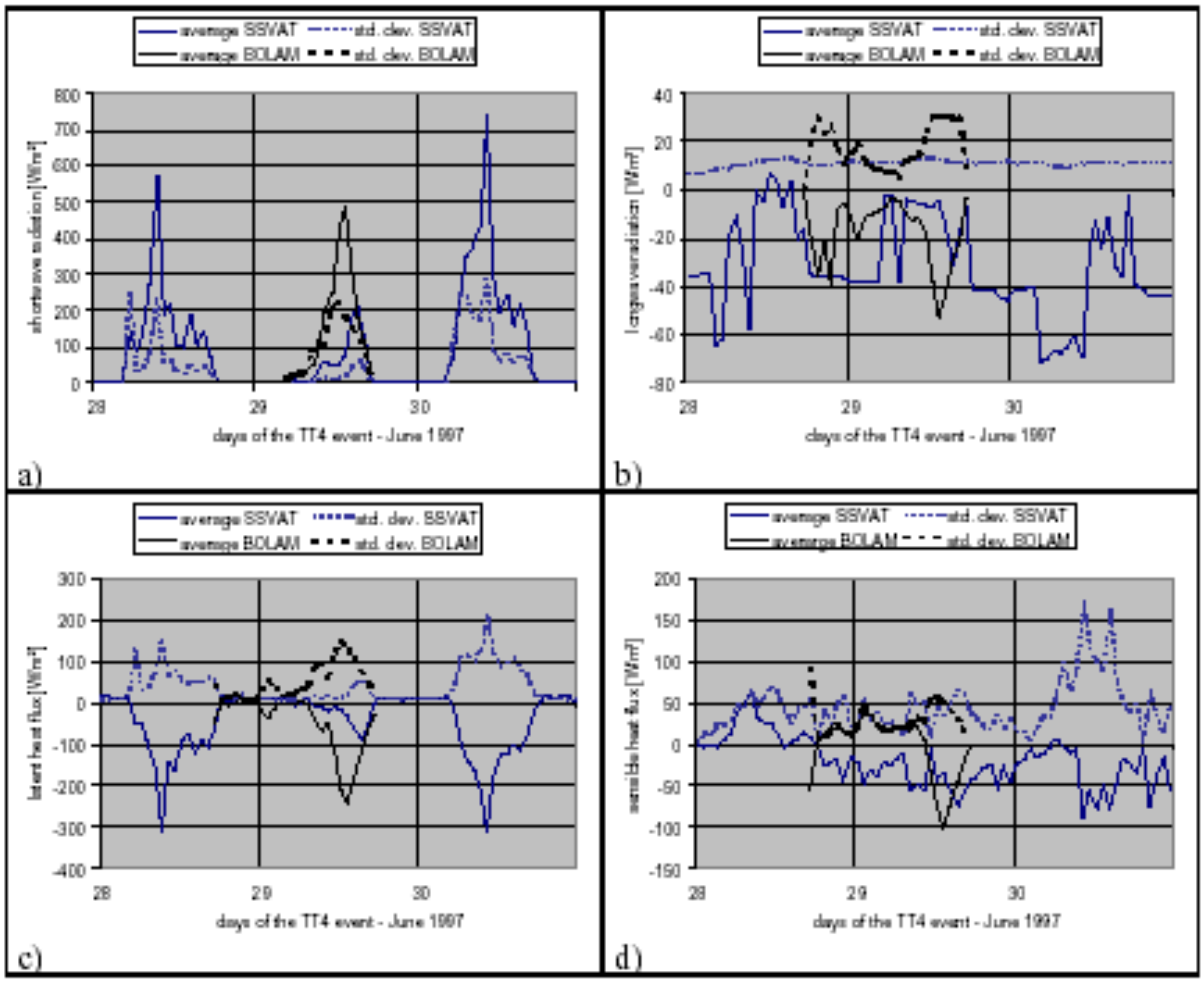

Fig. 4. *Catchment spatial average and spatial standard deviation of the distribution of the energy fluxes simulated by BOLAM (thick lines) and SSVAT (thin lines) during the TT4 event: a) shortwave radiation balance, b) longwave radiation balance, c) latent heat, d) sensible heat.*

Table 2. Descriptive statistics of the catchment average energy fluxes simulated by the hydrological model SSVAT and the meteorological model (BOLAM); the period of time starts at 18:00 UTC of the 28th of June and ends at 18:00 UTC of the 29th of June 1997 (TT4 event). All the values are expressed in W m^{-2}, except for the sum which is expressed in MJ m^{-2}.

	shortwave radiation		**longwave radiation**		**latent heat**		**sensible heat**	
	SSVAT	*BOLAM*	*SSVAT*	*BOLAM*	*SSVAT*	*BOLAM*	*SSVAT*	*BOLAM*
average	*33.6*	***86.9***	*-22.8*	***-17.9***	*-10.4*	***-49.7***	*-32.5*	***-3.3***
st. deviation	*56.7*	141.6	*15.2*	14.2	*28.9*	70.9	*20.2*	38.5
sum	*3.0*	*7.82*	*-2.0*	*-1.6*	*0.9*	*-4.47*	*-2.9*	*-0.30*

Table 3. Coordinates of target stations.

Station	***Company***	***Long.***	***Lat.***	***E UTM***	***N UTM***	***h [m a.s.l.]***
Domodossola-Siberia	CNR-ISIATA	8.290	46.092	445105	5104397	252
Domodossola-Nosere	Piedmont Region	8.279	46.099	446089	5105831	252

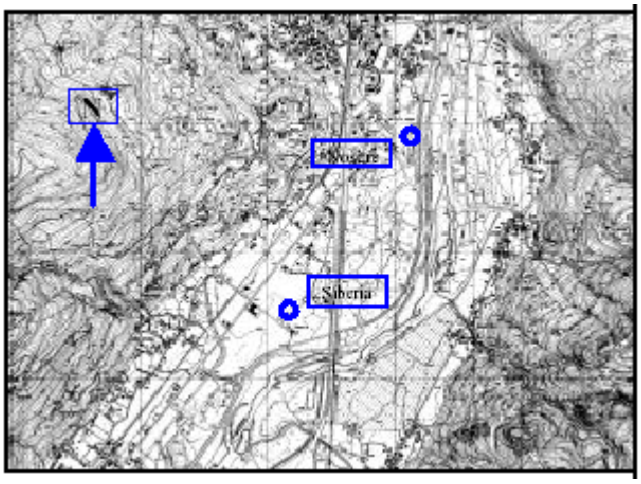

Fig. 5. *Location of the target stations (from CTR maps n. 051080 and 051120 Piedmont Region) – 1 km grid.*

Fig. 6. *CNR site at Domodossola-Siberia. Houses are located to the east of the 7 m mast.*

THE DOMODOSSOLA TEST SITE

The Domodossola-Nosere station is part of the meteorological automatic network operated by the Hydrometeorological Service of Piedmont Region. Hourly data of air temperature, relative humidity, pressure, precipitation, wind speed and incoming solar radiation are recorded continuously. Average and extreme values of the time series starting at hour 1 of the first day of the Special Observing Period (SOP) —1.9.99, and ending at the hour 24 of the last SOP day — 15.11.99 are listed in Table 4. For the distributed event simulations, such as the TT4 event discussed in the previous paragraph, the Nosere station (Fig. 1 and Table 1) was chosen as representative for the whole basin as far as solar radiation and air pressure are concerned. For the Isorno sub-basin and for the area at the bottom of the Toce valley, the data series of precipitation, air temperature and humidity measured at Nosere were also input to the distributed simulation.

The Domodossola-SIBERIA micro-meteorological station was a temporary experimental station managed by the national research council, CNR (Falappi *et al.*, 2001b). The station was installed in a cultivated area, where the height of the vegetation changed slightly during the experiment (Fig. 6). The higher obstacles to the wind flux are mainly in the crosswind directions; thus, they could not perturb the main flows along the valley. The instruments were installed on two masts, 2 m and 7 m high, respectively. Monitored variables were: mean wind speed (U) and direction (Dir), sonic temperature (T_s), standard deviations of velocity components (σ_u, σ_v, σ_w), momentum flux ($\overline{u'w'}$), kinematic heat flux ($\overline{w'T'_s}$), air temperature (T_{air}) and relative humidity (RH); surface soil temperature (T_{ss}); soil temperature at different depths: z=–1; -5; –10; –17; –25 and –50 cm (Tg_z) and heat flux into the ground (G); solar incoming radiation ($GR\downarrow$); all wavelength incoming ($AW\downarrow$) and outgoing radiation ($AW\uparrow$). The data acquisition from the micro-meteorological station started at 09.45 a.m. on 13 September 1999 and ended at 10.00 a.m. on 12 November 1999. Average and extreme values of the recorded time series of the soil temperature at different depths and of the air temperature and humidity are listed in Table 5, while Table 6 shows the average and the extreme values of the other monitored variables.

The time series of observations recorded by the two

Table 4. Statistics of the meteorological variables measured at Nosere, during the experiment period (* = total amount).

NOSERE	*RH* *[%]*	T_{air} *[°C]*	*tpr* *[mm/h]*	*P* *[hPa]*	*GR↓* *[W/m²]*	U_{10m} *[m/s]*
Mean	86.57	13.49	0.26 (466.8*)	991.92	96.10	1.03
Max	100.00	28.70	21.00	1004.50	814.00	7.46
Min	29.00	0.10	0.00	973.50	0.00	0.00

Table 5. Statistics of data from thermo-hygrometer and thermo-resistances at Siberia (several data are missing in the T_{-25} time series).

	RH (%)	*T* (°C)	*Tsurf* (°C)	T_{-1} (°C)	T_{-5} (°C)	T_{-10} (°C)	T_{-17} (°C)	T_{-25} (°C)	T_{-50} (°C)	$\overline{T_{0-24}}$ (°C)
Mean	84.72	11.11	11.13	13.78	12.45	14.40	13.02	18.65	15.27	12.64
Max	99.65	24.50	30.61	30.50	20.66	24.76	18.02	22.37	20.71	18.86
Min	24.64	-0.37	-0.60	4.55	6.19	6.79	7.62	16.07	10.07	6.80

Table 6. Statistics of Starpyranometer, Pyrradiometer and Hukseflux data.

	SW↓ (W m^{-2})	AW↓ (W m^{-2})	AW↑N (W m^{-2})	T_r (AW↓–AW↑)	G (K)	(W m^{-2})
Mean	82.29	429.65	391.19	38.46	12.61	-1.61
Max	833.91	1244.59	593.30	657.33	32.77	106.31
Min	0.00	262.25	306.33	-112.97	-1.87	-38.07

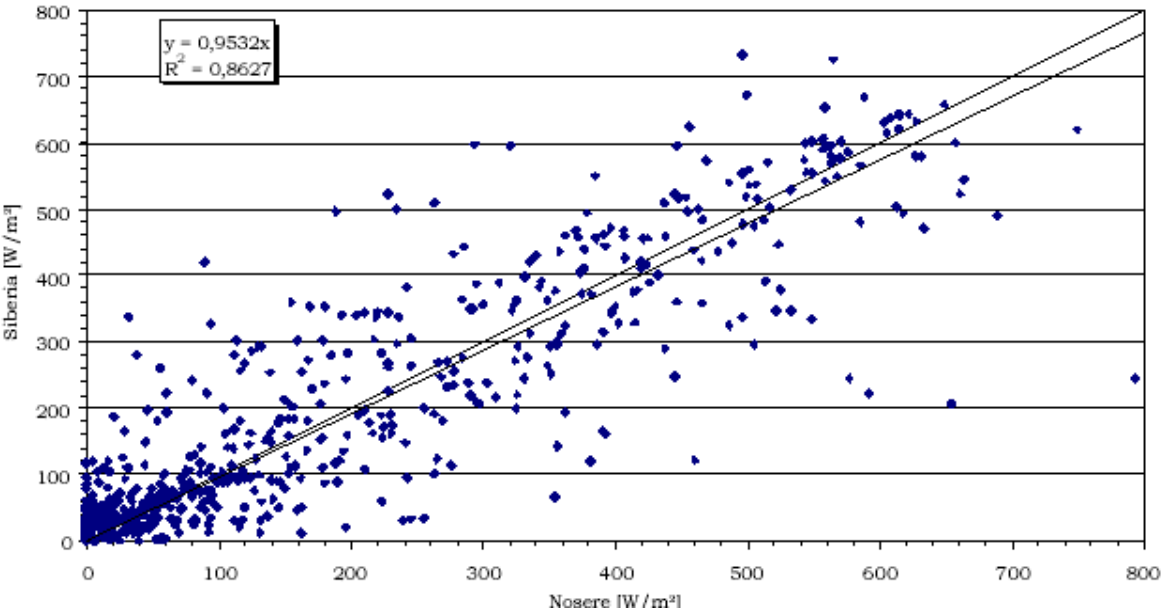

Fig. 7. *Solar radiation, SW↓, measured at Siberia and at Nosere.*

Table 7 – *Statistics of the deviations between time series recorded at Siberia and homogeneous time series observed at Nosere*

SIBERIA *v.* NOSERE	ΔRH (%)	ΔT_{2m} (°C)	ΔSW↓ (W m^{-2})	ΔU_{10m} (m s^{-1})
Mean	0.65	0.62	-13.81	-0.16
Max	0	-1.2	19.91	0.22
Min	-1.86	2.53	-0.5	0.01

stations for the same variable are highly correlated, as shown for example in Fig. 7, which is a scatter plot of incoming shortwave radiation time series recorded by the two series. The incoming solar radiation recorded at Siberia is lower than that measured at Nosere and the mean difference is about 13.8 W m^{-2}, as shown in Table 7. This systematic deviation might be due to local microclimatic differences between an urban and a rural area. Nevertheless, the differences between the recordings at the two stations are sufficiently low to allow the use of the data measured at Nosere, corrected on the basis of the results of the linear regression analysis, to substitute for data missing at the Siberia station.

SIMULATION OF THE ENERGY FLUXES AT SIBERIA

The energy fluxes at the land surface-atmosphere interface were simulated for the Domodossola test site by applying the SSVAT model using the standard meteorological data as input. Micro-meteorological observations at Siberia were used for the validation of model results. Missing data for the Siberia site were reconstructed on the basis of the spatial correlation with observations at Nosere. Precipitation, air pressure and wind velocity data recorded at Nosere were used for the simulation without any corrections, since those variables were not measured at Siberia.

For each time step (1 h), if soil temperature data measured at Siberia were available, they were used as input to the model; if not, the soil surface temperature was computed by the model, as described above. The comparison between soil temperature measured and computed by the model is shown in Fig. 8. Measured temperature was actually computed on the basis of observations for the first 17 cm underneath the soil surface.

The vegetation was assumed to consist of bushes in the autumn season, having an albedo just a little lower than that of grassland (α =0.23). Accordingly, the following values for the Leaf Area Index, the mean height of vegetation and the albedo were chosen: $LAI = 1$, $h_{0c} = 0.5$ m, $\alpha = 0.18$ (see also Gurtz *et al.*, 1999).

The albedo was actually estimated from incoming and allwave outgoing radiation observations, since the temperature of the soil surface was known. In fact, albedo is defined as equal to the ratio between reflected solar radiation and incoming solar radiation, which in this case is known. To estimate the reflected solar radiation, total radiation has to be decreased by thermal radiation from the Earth, which is a function of surface temperature. The albedo can, therefore, be estimated at each time step. Limiting the analysis to the hours around midday, when the incoming radiation reaches the highest values in the day (generally higher than 300 W m^{-2}), an average value of 0.18 was found.

Also, the parameters describing the soil were carefully estimated to represent the point characteristics of the Siberia site (Falappi, 2000). The damping factor γ was evaluated by taking the average of the damping factor of the amplitudes

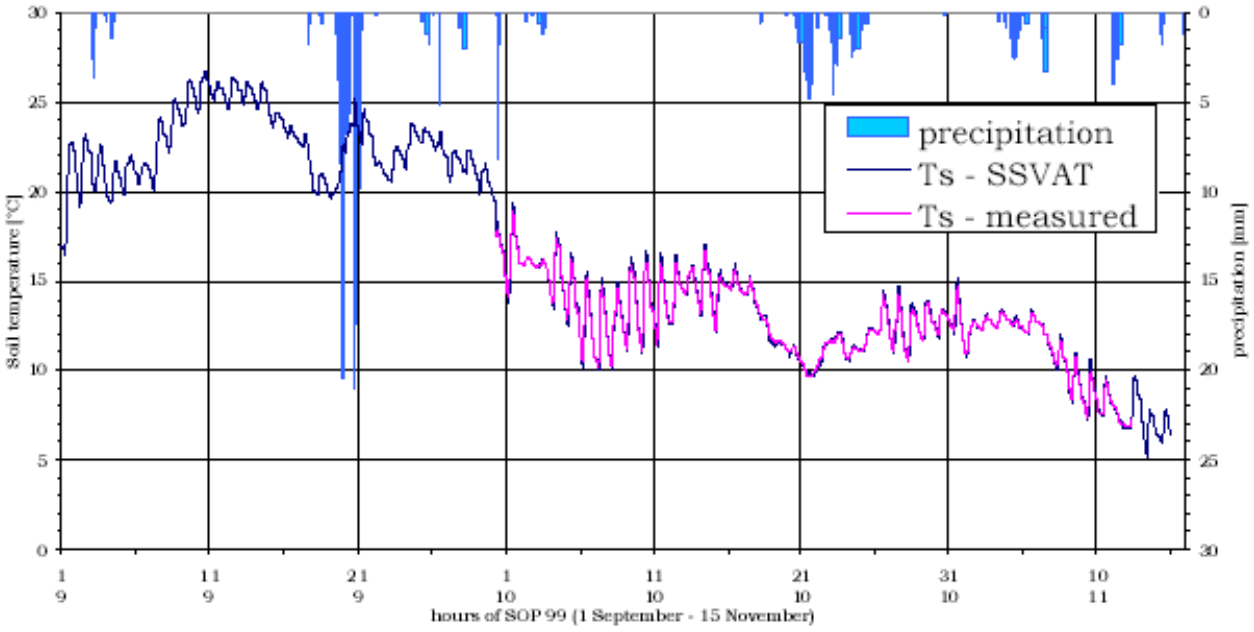

Fig. 8. *Comparison between soil temperature measured at the Siberia site and computed by the SSVAT model for the corresponding cell; "tpr" is the measured total precipitation.*

and the damping factor of the phases of the temperature profile. For the computation of the thermal diffusion α_s the following expression was used $\alpha_s = \pi/(\gamma^2 \tau)$. The soil conductivity λ was finally derived by inverting the relationship between heat flux into the ground and the vertical temperature gradient. Two different sets of values were defined, one for dry soil (without precipitation) and another one for wet soil (with precipitation), assuming that the soil was mainly of the sandy-loam type, as confirmed by field and laboratory soil measurements carried out during MAP-SOP (Falappi *et al*., 2001a):

Dry soil	**Wet soil**
λ = 0.603 W/(m °C)	λ= 1.676 W/(m °C)
γ = 7.2 m^{-1}	γ = 12 m^{-1}
$\alpha_s = 0.701\times10^{-6}$ m²/s	$\alpha_s = 0.253\times10^{-6}$ m²/s

THE ESTIMATE OF THE LATENT HEAT

A qualitative estimate of the latent heat flux ($\lambda_e E$) was also derived, as a residual, from a simplified equation of the energy balance at the surface. If R is the net radiation, H_g is the heat flux into the ground and H_s is the sensible heat flux, then:

$$\lambda_e E = -H_l = R + H_s + H_g$$

Each term on the right-hand side of the energy balance equation is either observed or can be evaluated directly from observations of related quantities, that is, by using measured turbulent quantities. Then the latent heat flux can be estimated, but obviously any error in the measurements affects this estimate.

If the 'eddy correlation' procedure is applied, the sonic anemometer estimates the quantity $\overline{w' T_s}$, that is the average of the product of the fluctuating component of the vertical wind velocity, w', and the fluctuations of the sonic temperature T_s' (Falappi *et al*., 2001b). This estimate is actually affected by the water vapour content of the air and, therefore, it differs from the turbulent sensible heat flux, $\overline{w' T'}$, where T' is the fluctuating component of the air temperature. Further correction is needed to take account of the velocity component normal to the transmitter-receiver axis. Finally, the sensible heat flux can be computed on the basis of the following equation (Schotanus *et al.*, 1983; Kaimal and Gaynor, 1991):

$$\overline{w'T'} = \overline{w'T_s'} + 2T \cdot U \cdot \frac{\overline{u'w'}}{C^2} - 0.51 \cdot T \cdot \overline{w'q'}$$

where U is the horizontal wind velocity and C is the sonic velocity. The covariance $u'w'$ is related directly to the friction velocity u*, as stated in the following expression:

$$\overline{u'w'} = -u_*^2$$

minus being the usual sign in the surface layer of the horizontal momentum flux. The sonic velocity is given as a function of the air temperature expressed in K:

$$C = 20.034\sqrt{T} \quad \text{m s}^{-1}$$

If measurements of the vapour turbulent flux, $w'q'$, are not available, a simplified relationship is used:

$$\overline{w'\theta'} = \overline{w'T_s'} + 2T \cdot U \cdot \frac{\overline{u'w'}}{C^2}$$

which is correct when the humidity is low, but introduces an error (≈10%) in the estimate of sensible heat flux in these experimental conditions.

Finally, to express simulated and observed quantities in the same measurement units, the kinematic flux has to be multiplied by the air density ρ_a and the specific heat at constant pressure at standard conditions c_p.

As the data examined were raw, no detrending procedure or filtering technique was applied and so they could have been affected by errors due to the atmospheric non-stationary conditions (wind acceleration and deceleration, rotation). Notwithstanding, it is preferable to study raw data in the first place and to apply the corrections afterwards and, also, to take account of the information given by low frequency values. The detrending correction could sometimes eliminate behaviour typical of complex terrain. Non-spectral filtering could induce perturbations at any frequency. As far as the radiation fluxes are concerned, the model results agree with observations, as do those for shortwave radiation. On the other hand, the two series of simulated and observed sensible heat flux show a systematic shift, perhaps induced by a shift in the simulated and observed soil temperatures.

Nevertheless, the estimate of the latent heat flux derived from micro-meteorological measurements is very similar to the simulated flux, even if a bit lower during daylight and higher during the night (Fig. 9). Actually, the model computes the potential evapotranspiration without considering the control induced by the soil moisture content. In fact, differences between the two estimates during the day are higher in dry periods, since in the simulation period (September–October) several rainfall events kept the soil wet (Falappi *et al*., 2001b). As shown in Table 4, total precipitation observed during Map-SOP'99 was about 467 mm. Also, vegetative cover (grass) at the site transpires strongly during the day, while at night condensation can recharge soil moisture which is always high early in the morning.

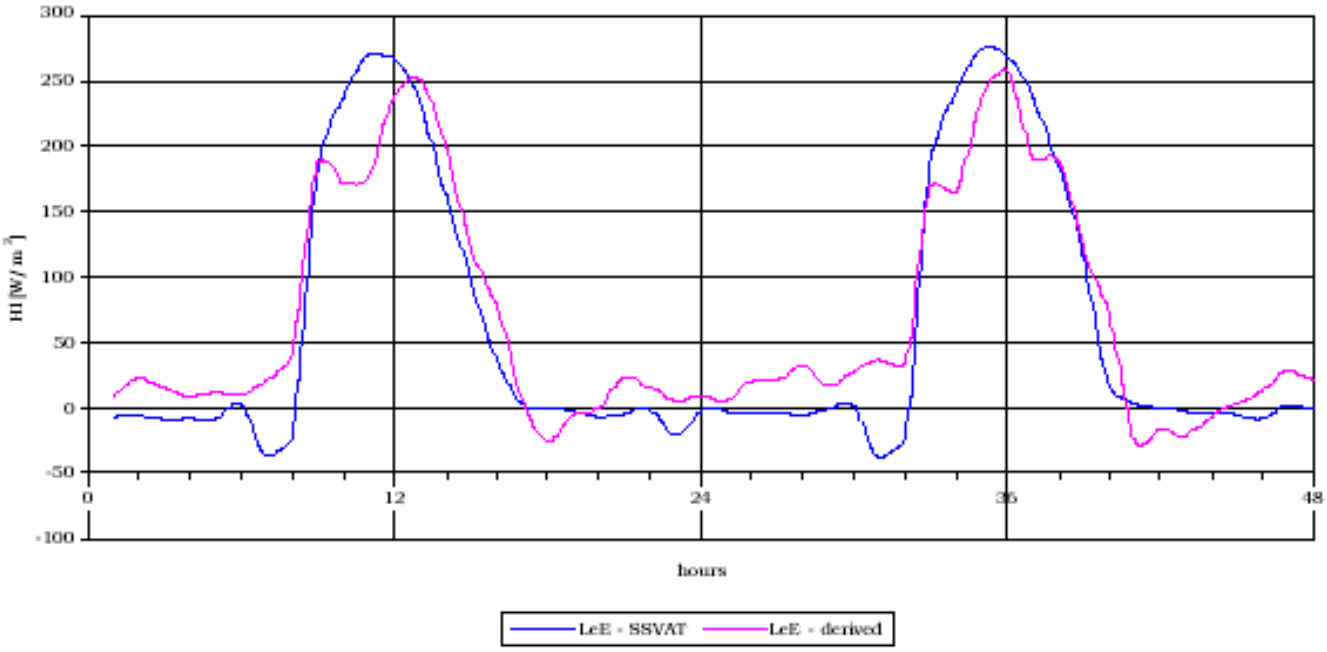

Fig. 9. *Latent heat derived from turbulent measurements and simulated by the SSVAT model – period: 8-9 October 1999.*

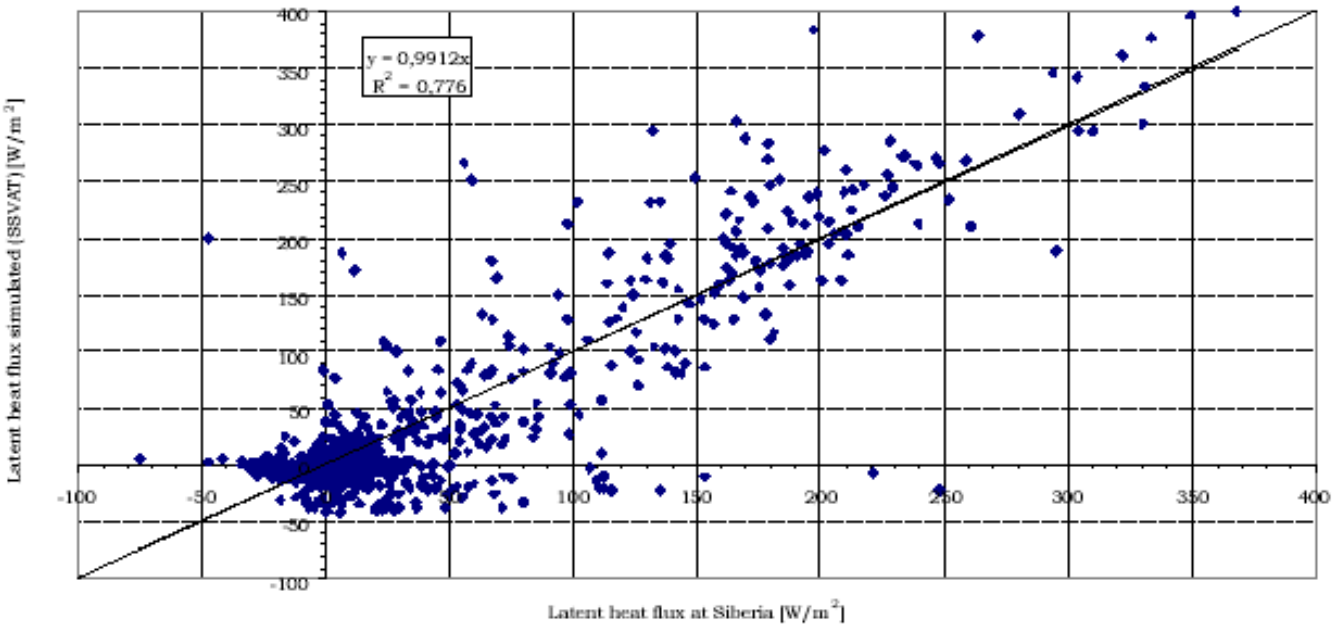

Fig. 10. *Latent heat derived from turbulent measurements and simulated by the SSVAT model – MAPSOP*

The night-time behaviour seems to be the opposite for the two estimates of latent heat. The micro-meteorological estimate shows a minimum after sunset and then increases until the early hours of the morning, while the simulated flux minimum occurs just before sunrise. The simulated behaviour seems to be more realistic, since the minimum flux shows the same timing of the minimum of air and soil temperature and of radiation. Figure 10 is a scatter plot of the simulated latent heat flux versus 'estimated' latent heat flux for the whole MAP-SOP (1.9.99–15.11.99), showing good correlation (R^2=0.78).

ABOUT THE SURFACE ROUGHNESS VALUE

Part of the analysis concerned the aerodynamic determination of the surface roughness, z_0, from data taken at a single level. If the quantity $kU(z)/u^* = \psi_m(z/L, z_0/L)$ is plotted versus z/L, where L is the Monin-Obukhov length scale, the asymptotic value of the similarity function ψ_m for $z/L \rightarrow 0$ can be found, i.e. for near-neutral conditions ($|L|>200$m) (Trombetti and Tagliazucca, 1994). Following the parameterisation by Dyer (1974), the wind profile can be expressed using the following relationship:

$$U = u^*/\ln(z/z_0) + \beta(z-z_0)/L$$

If the linear term is not considered, the aerodynamic expression of the roughness can be derived:

$$z_0 = z \exp[-k/u^* U(z)]$$

Measurements recorded during the MAP-SOP 99 show that the atmospheric circulation in the surface layer at the Siberia site was directed mainly along the valley axis (south-north), and the strength of the cross-valley winds was generally very low (<1 m s^{-1}). North winds (down into the valley) are few and are associated with a very low value of z_0, five times lower than that associated with south winds (up the valley); obstacles to the flux from the south perhaps increase air turbulence and, therefore, the value of the aerodynamic roughness. Accordingly, the down-valley flux observed by Steiner *et al*. (2002) at Pieve Vergonte, a few kilometres downstream of Domodossola, was not often observed at Siberia. In fact, horizontal inhomogeneity can seriously affect the turbulence profile in the near surface layer, as assessed by Andretta *et al*. (2000, 2001).

The mean arithmetic roughness length for winds along the valley axis is 0.176±0.10 m, somewhat higher than might be expected for typical farmland. The scatter diagram of z_0 versus z/L shows that the average value is representative of the whole set of values. The large standard deviation might be due to the spatial variability of sparse roughness elements (buildings and trees) and obstacles (hubs, roads, etc.) that interfere with the flow along slightly different trajectories.

The best simulation of the latent heat flux was actually obtained with 'standard' roughness values, that is $z_0 = 0.1\ h_c$, as suggested in the literature. In fact, the aerodynamic estimate for south and north winds described previously overestimates the latent heat flux. Descriptive statistics of the micro-meteorological estimate of the latent heat flux are reported in Table 8, together with the statistics of the simulated flux with both roughness values. Although the two simulated fluxes are different, the correlation coefficient between the two series is higher than 0.8, implying in each case a good correlation between observations and simulations.

Conclusions

A distributed Snow-Soil-Vegetation-Atmosphere Transfer (SSVAT) model was developed and applied to simulate the energy fluxes at the land surface-atmosphere interface in the Toce Valley during some selected events. For the event of June 1997, the SSVAT-simulated energy fluxes were comparable to those simulated by the meteorological model BOLAM. On average, the energy terms simulated by the two models were similar, even if the exchange processes were quite sensitive to the surface characterisation and to local meteorological conditions, which are difficult to represent at the mesoscale.

The SSVAT model was further tested at the point scale by simulating the energy fluxes for the MAP-Special Observing Period. Simulated turbulent fluxes were compared to turbulent quantities derived from micro-meteorological observations recorded at the Domodossola test site. The model simulated potential ET, that approximated the effective ET derived from turbulence measurements: cumulative quantities for the whole special observing period differed by about 12% (Fig. 11). In fact, in autumn, evaporative fluxes could be at the potential rate, because the soil moisture was quite high and close to field capacity.

Table 8 – *Statistics of the observed and simulated latent heat flux at Siberia, 1.9.99 – 15.11.99. Two different values of surface roughness are assumed for the simulation.*

[W/m²]	***CNR***	***SSVAT*** $z_0 = 0.1\ h_c$	***SSVAT*** $z_0 = 0.176$	*ΔCNR-SSVAT* $z_0 = 0.1\ h_c$	*ΔCNR-SSVAT* $z_0 = 0.176$
Mean	40.7	43.8	69.3	-3.09	-28.61
Max	365.27	424.9	564.3	-59.63	-199.03
Min	-74.1	-53.2	-36.9	-20.89	-37.19
St. dev.	72.0	96.5	115.0		
Correlation		0.882	*0.859*		

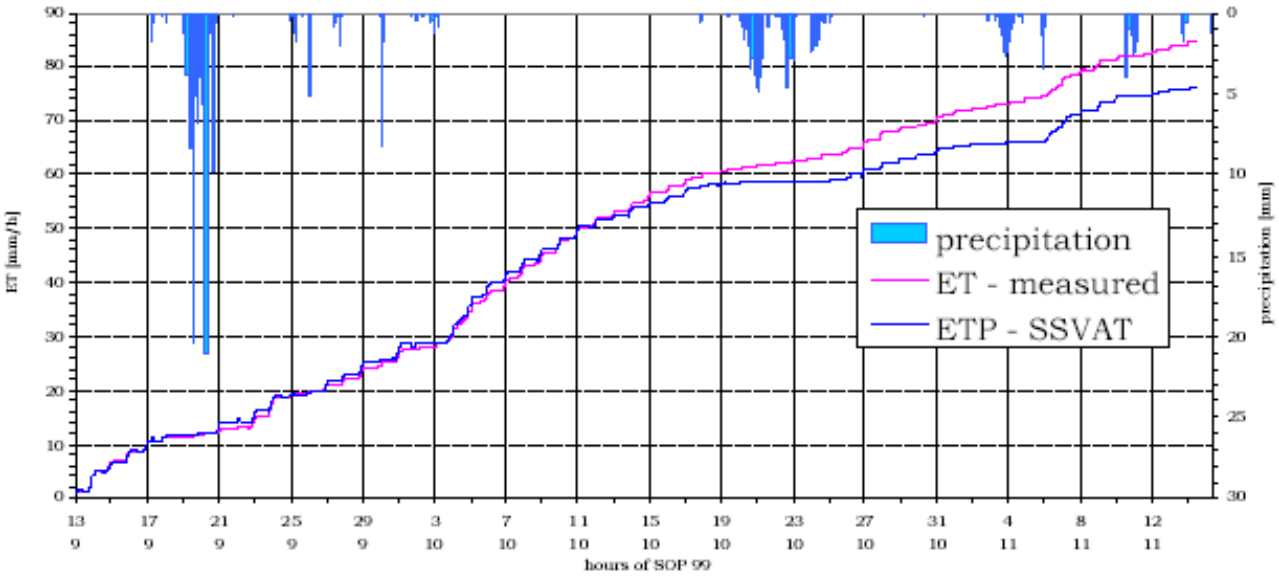

Fig. 11. *Cumulated evapotranspiration measured and simulated at Siberia during the TOCEX experiment.*

The deviation between the two curves might be due either to the estimated values of the parameters describing the soil (which are different for wet and for dry soil) used in the model simulation (blue line), or to the errors affecting measured energy terms from which the estimate of the latent heat flux was derived (pink line).

Further studies concerned the estimate of the roughness length, upon which the wind profile is defined. The aerodynamic estimate provided higher values than expected for the type of soil and land use considered, resulting in higher values of the simulated latent heat flux but keeping a good correlation between the two estimates of the turbulent flux. This result confirms the value of traditional meteorological observations, but it also outlines the relevance of innovative monitoring techniques, aimed at traditional data validation.

Acknowledgements

This research was developed in the framework of the EU funded RAPHAEL project, contract ENV 4-CT97-0552, and of the CNR-GNDCI VAPI-RIVERS project. The authors acknowledge Settore Meteoidrografico of Regione Piemonte, for making their automatic hydrometeorological dataset available, Dr. Andrea Buzzi (CNR-ISAO) and Dr. Mauro Tagliazucca (CNR-ISAO) for scientific support in meteorological modelling, Prof. Baldassare Bacchi (University of Brescia) and Prof. Roberto Ranzi (University of Brescia) for advice during the development of the project.

References

Andretta, M., Zimmermann, S., Rotach, M.W., Calanca, P., Christen, A. and Vogt, R., 2000. Investigation of the near-surface boundary-layer in an Alpine valley. *MAP newsletter* 13, 68–69.

Andretta, M., Weiss, A., Kljun, N. and Rotach, M.W., 2001. Near-surface turbulent momentum flux in an Alpine valley: observational results. *MAP newsletter 15*, 122–125.

Bach, H. and Braun, M., 1999. Fuzzy logic classification for the extraction of surface parameters in Alpine areas. *Proc. IGARSS.*

Bacchi, B. and Ranzi, R., 2003. The Raphael project: an overview. *Hydrol. Earth Syst. Sci.*, **7**, 784–798.

Benoit, R., Buzzi, A., Binder, P., Cosma, S., Kaufmann, P. and Richard, E., 2000. Meteorological simulations of some heavy precipitation events. In: *Runoff and atmospheric processes for flood hazard forecasting and control (RAPHAEL).* Contract ENV4-CT97-0552, Final Report, Brescia, Italy.

Biancotti, A., Bellardone, G., Bovo, S., Cagnazzi B., Giacomelli, L. and Marchisio, C., 1998. *Distribuzione regionale di piogge e temperature, Regione Piemonte, Torino.*

Bougeault, P., Binder, P., Buzzi, A., Dirks, R., Houze, R., Kuettner, J., Smith, R.B., Steinacker, R. and Volkert, H., 2001. The MAP Special Observing Period. *Bull. Amer. Meteorol. Soc.*, **82**, 433–462.

Buzzi, A., Fantini, M., Malguzzi, P. and Nerozzi, F., 1994. Validation of a Limited Area Model in cases of mediterranean cyclogenesis: surface fields and precipitation scores. *Meteorol. Atmos. Phys.*, **53**, 137–153.

Ca' Zorzi, F. and Dalla Fontana, G., 1986. Improved utilization of maximum and minimum daily temperature in snowmelt modelling. *IAHS Publication no. 155.*

Calder, I.R., 1990. *Evaporation in the Uplands*.Wiley, Chichester, UK.

Colbeck, S.C. and Anderson, E.A., 1982. The permeability of a melting snow cover. *Water Resour. Res.*, **18**, 904–908.

Falappi, L., 2000. *La valutazione dell'evapotraspirazione in ambienti montani.* Ph.D. thesis, Politecnico di Milano.

Falappi, L., Barontini, S., Clerici, A., Grossi, G., Savoldi, E. and Ranzi, R., 2001a. *Field and laboratory soil measurements in the Toce Valley (Italy), during the MAP-SOP 1999 TOCEX experiment.* Technical Report, R. Ranzi and B. Bacchi (Eds.), Dipartimento di Ingegneria Civile dell'Università di Brescia, Italy. 10.III.

Falappi, L., Giostra, U. and Tagliazucca, M., 2001b. *Measurements of turbulent fluxes in the surface layer in the Domodossola-Siberia site during MAP-SOP 1999 TOCEX experiment.* Technical Report. R. Ranzi and B. Bacchi (Eds.), Dipartimento di Ingegneria Civile dell'Università di Brescia, Italy. 10.XI.

Grossi, G., 1996. *Un modello idrologico distribuito della dinamica del manto nevoso: teoria ed applicazioni*. Ph.D. thesis, Politecnico di Milano.

Grossi, G., Lettenmaier, D.P. and Rosso, R., 1995. The effect of DEM resolution on a distributed energy balance snow accumulation and ablation model (abstract). *Annales Geophysicae*, Supplement II to Volume 13, Part II, *Proc. XX General Assembly European Geophysical Society*, Hamburg, 3–7 April 1995, C435.

Grossi, G., Bacchi, B., Gagni, F. and Ranzi, R., 2001. *Hydrometeorological monitoring in the Toce Valley (Italy), during the MAP-SOP 1999 TOCEX experiment*. Technical Report, R. Ranzi and B. Bacchi (Eds.), Dipartimento di Ingegneria Civile dell'Università di Brescia, Italy. 10.VIII.

Gurtz, J., Baltensweiler, A. and Lang, H., 1999. Spatially distributed hydrotope-based modelling of evapotranspiration and runoff in mountainous basins. *Hydrolog. Process.*, **13**, 2751–2778.

Kaimal, J.C. and Gaynor, J.E., 1991. Another look at sonic anemometer. *Bound. Layer Meteorol*., **56**, 401–410.

Malguzzi, P. and Tartaglione, N., 1999. An economical second order advection scheme for explicit numerical weather prediction. *Quart. J. Roy. Meteorol. Soc.*, 125, 2291–2303.

Monteith, J.L., 1981. Evaporation and surface temperature. *Quart. J. Roy. Meteorol. Soc*., **107**, 1–27.

Obled, C. and Harder, H., 1978. A review of snowmelt in the mountain environment. *Proc. Int. Conf. Modelling of Snow Cover Runoff*, S.C. Colbeck and M. Ray, CRREL (Eds.), Hanover, New Hampshire, USA. 26–28.

Pilotti, M., Gandolfi, C. and Bischetti, G.B., 1996. Identification and analysis of natural channel networks from digital elevation models. *Earth Surf. Process. Landforms*, **21**, 1007–1020.

Ranzi, R. and Bacchi, B. (Eds.), 2000. *Hydrological aspects in the Mesoscale Alpine Programme-SOP experiment*. Dept. of Civil Engineering, Univ. of Brescia, Italy. Technical Report, 10.

Ranzi, R. and Rosso, R., 1990. A physically based distributed snowmelt-runoff model for a small alpine basin (abstract). *Proc. XV General Assembly European Geophysical Society*, Copenhagen, 23–27 April, *Annales Geophysicae*, Special Issue, 91.

Ranzi, R. and Rosso, R., 1991. A physically based approach to modelling distributed snowmelt in a small alpine catchment. *IAHS Publication no. 205*, 141–150.

Ranzi, R., Grossi, G. and Bacchi, B., 1999. Ten years of monitoring areal snowpack in the Southern Alps using NOAA-AVHRR imagery, ground measurements and hydrological data. *Hydrolog.Process*., **13**, 2079–2095.

Schotanus, P., Nieuwstadt, F.T.M. and De Bruin, H.A.R., 1983. Temperature measurement with a sonic anemometer and its application to heat and moisture fluxes. *Bound. Layer Meteorol.*, **26**, 81–93.

Schulla, J., 1997. Hydrologische Modellierung von Flussgebieten zur Abschätzung der Folgen von Klimaänderungen. *Zürcher Geographische Schriften 69*, Geographisches Institut ETH, Switzerland.

Steiner, M., Bousquet, O., Houze, R.A., Smull, B.F. and Mancini, M., 2003. Airflow within major alpine river valleys under heavy rainfall. *Quart. J. Roy. Meteorol. Soc.*, in press.

Wigmosta S.M., Lance, W.L. and Lettenmaier, D.P., 1994. A distributed hydrology vegetation model for complex terrain. *Water Resour. Res.*, **30**, 1665–1679.